

A parameteric class of composites with a large achievable range of effective elastic properties

Igor Ostanin^{1a}, George Ovchinnikov^a, Davi Colli Tozoni^b, Denis Zorin^{a,b}

^a*Skolkovo Institute of Science and Technology, Nobel St. 3, Moscow, 143026, Russia*

^b*New York University, 719 Broadway, New York, 10003, USA*

Abstract

In this paper we investigate numerically an instance of the problem of *G-closure* for two-dimensional periodic metamaterials. Specifically, we consider composites with isotropic homogenized elasticity tensor, obtained as a mixture of two isotropic materials, focusing on the case of a single material with voids. This problem is important, in particular, in the context of designing small-scale structures for metamaterials in the context of additive fabrication, as this type of metamaterials makes it possible to obtain a range of material properties using a single base material.

We demonstrate that two closely related simple parametric families based on the structure proposed by O. Sigmund in [20] attain good coverage of the space of isotropic properties satisfying Hashin-Shtrikman bounds. In particular, for positive Poisson ratio, we demonstrate that Hashin-Shtrikman bound can be approximated arbitrarily well, within limits imposed by numerical approximation: a strong evidence that these bounds are achievable in this case. For negative Poisson ratios, we numerically obtain a bound which we hypothesize to be close to optimal, at least for metamaterials with rotational symmetries of a regular triangle tiling.

1. Introduction

The relationship between the geometric structure of a periodic composite material and its effective properties (elastic properties in particular) is a central question in mechanics of composites. The direct problem – finding the effective elastic properties from the known periodic structure of the composite material – is solved by means of homogenization theory. The inverse problem (finding a periodic structure yielding specific material properties) is more challenging: in general, it requires solving a non-convex non-linear PDE constrained optimization problem with highly nonunique solution (inverse homogenization). Most importantly, it is not known when this problem has feasible solutions, *i.e.*, for which target elasticity tensors a corresponding composite structure with a given base material exists. This problem is known as the *G-closure* problem [1]. While for the heat conduction explicit solutions are known in some cases, for elasticity this is a long-standing problem. The outer bounds of the feasible region in the space of elasticity tensors are given by the well-known Hashin-Shtrikman bounds [7] on the bulk and shear moduli, as well as their refinement [2]. While it is known that the *extremal* points on the boundaries are achievable by sequential laminates (*i.e.*, shear and bulk modulus can be simultaneously maximized or minimized), less is known about the rest of the region: *e.g.*, how closely one can approach the extremal bulk modulus given a fixed shear modulus. These extreme solutions are given by sequential laminates, *i.e.*, assuming infinite geometric complexity and separation of scales (*i.e.*, very large differences in periods of laminations in sequence), so are not practical, although one can manufacture, with considerable difficulty, finite-resolution approximations of these materials.

We explore solutions to this problem numerically, using specific parametric families of structures inspired by several previous papers. While the geometric complexity of the structures in these families increases,

¹Corresponding author, tel: +79150174677, e-mail: i.ostanin@skoltech.ru

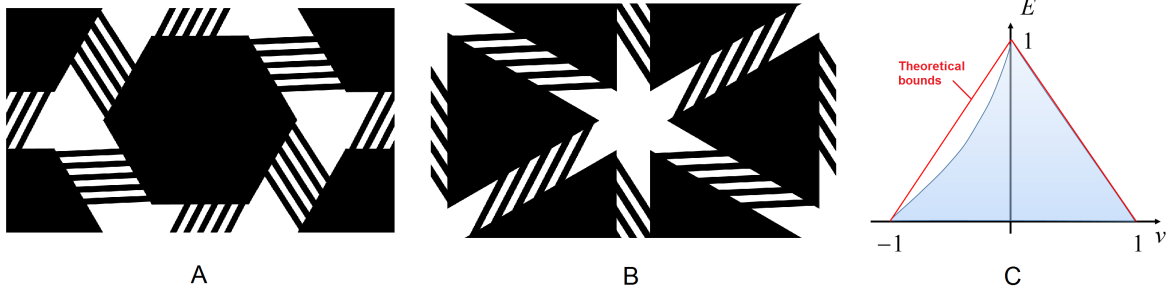


Figure 1: (A,B) parametric structure families, (C) Domains of achievable effective elastic properties and Hashin-Shtrikman theoretical bounds ($E_b = 1$, $\nu_b = 0$) in (E, ν) domain.

as we approach the bounds, we show that with modest geometric complexity, and no separation of scales, one can approach the boundaries closely. Thus, a large fraction of our structures, can be, in principle manufactured and can serve as a starting point for further simplification.

Contributions. We explored two families of structures (depicted in Figure 1(A, B)), using a hexagonal base cell, and symmetric with respect to rotation of the cell on $\frac{n\pi}{3}$, which ensures that their effective elastic tensors are perfectly isotropic. Each structure has only four parameters. We observe that these structures have the following properties:

- For positive Poisson ratio, the bounds of the Hashin-Shtrikman region are approached arbitrarily closely, within limits of numerical accuracy.
- For negative Poisson ratio, chirality parameter allows us to cover a larger fraction of the region defined by Hashin-Shtrikman bound than all previously known.
- The low number of parameters of the structure allows for simple mapping of material parameters to structure parameters, potentially avoiding inverse homogenization entirely.
- We show that for volume fractions different from one, for positive Poisson ratios, proposed structures are also close to the Hashin-Shtrikman bounds.
- For negative Poisson ratios, we show evidence that our structures are also close to optimal, at least in the local sense, suggesting that Hashin-Shtrikman bounds may not be achievable.
- Our family of structures in 2D covers a larger fraction of the Hashin-Shtrikman domain.

Figure 1(C) shows the set of Young moduli and Poisson's ratios that could be achieved by tuning the parameters of structures (A) and (B), as related to the known theoretical bounds on these moduli (see the discussion in the next section).

Remark. To illustrate material property coverage, in most of our figures we use Young modulus-Poisson ratio coordinates, vs. bulk-shear modulus more commonly found in the literature: the distance in this space captures the differences in material behavior in a more intuitive way. We discuss the relationship between these two parameterizations of material properties below.

2. Background and related work

Bounds on elastic properties of isotropic materials. The elastic tensor characterizing properties of a periodic composite material is obtained by homogenization over a base cell of the composite structure (Section 4). In this work, we consider composite structures that are isotropic due to spatial symmetries of the base cell. Such composites can be described by two independent elastic moduli (bulk and shear moduli or Young modulus and Poisson ratio). The best known bounds for composite properties are Hashin-Shtrikman bounds [7]. In case of well ordered strong (κ_s, μ_s) and weak (κ_w, μ_w) phases ($(\kappa_s^{HS} - \kappa_w^{HS})(\mu_s^{HS} - \mu_w^{HS}) > 0$), the HS bounds are:

$$\begin{aligned} \kappa_l^{HS} &< \kappa < \kappa_u^{HS}, & \mu_l^{HS} &< \mu < \mu_u^{HS}, \\ \kappa_u^{HS} &= \kappa_s + \frac{1-\phi}{\frac{1}{\kappa_w - \kappa_s} + \frac{\phi}{\kappa_s + \mu_s}}, & \kappa_l^{HS} &= \kappa_w + \frac{\phi}{\frac{1}{\kappa_s - \kappa_w} + \frac{(1-\phi)}{\kappa_w + \mu_w}}, \\ \mu_u^{HS} &= \mu_s + \frac{1-\phi}{\frac{1}{\mu_w - \mu_s} + \frac{\phi(\kappa_s + 2\mu_s)}{\kappa_s + \mu_s}}, & \mu_l^{HS} &= \mu_w + \frac{\phi}{\frac{1}{\mu_s - \mu_w} + \frac{(1-\phi)(\kappa_w + 2\mu_w)}{\kappa_w + \mu_w}}. \end{aligned}$$

Figure 2 shows Hashin-Shtrickman bounds for void-material (A,B) and bimaterial (C,D) composites, in terms of bulk and shear moduli (A,C) and Young modulus and Poisson ratio (B,D) for arbitrary volume fractions $0 \dots 1$ and for several fixed volume fractions. These bounds are known not to be optimal the general case: Cherkaev-Gibiansky bounds are substantially tighter in general [2]. However, in the case when the weak phase has zero elastic tensor, these bounds exactly coincide with the Hashin-Shtrikman bounds. In terms of volume fraction, bulk and shear moduli of the base material ϕ , κ_b and μ_b the bounds on effective bulk moduli κ and μ in this case reduce to:

$$\begin{aligned} 0 &< \kappa < \kappa_u^{HS}, & 0 &< \mu < \mu_u^{HS}, \\ \kappa_u^{HS} &= \kappa_b + \frac{1-\phi}{-\frac{1}{\kappa_b} + \frac{\phi}{\kappa_b + \mu_b}}, & \mu_u^{HS} &= \mu_b + \frac{1-\phi}{-\frac{1}{\mu_b} + \frac{\phi(\kappa_b + 2\mu_b)}{\kappa_b + \mu_b}}. \end{aligned} \quad (1)$$

Expressing bulk and shear moduli as $\kappa = \frac{E}{2(1-\nu)}$, $\mu = \frac{E}{2(1+\nu)}$, one obtains the isotropic bounds in terms of Young modulus and Poisson ratio, forming a triangular region:

$$\begin{aligned} 0 &< E(\nu) < -2C_1\nu + 2C_1, & 0 &< E(\nu) < 2C_2\nu + 2C_2, \\ C_1 &= \frac{E_b}{2(1-\nu_b)} + \frac{E_b(1-\phi)}{\phi(1-\nu_b^2) - 2(1-\nu_b)}, & & \\ C_2 &= \frac{E_b}{2(1+\nu_b)} + \frac{1-\phi}{\phi\frac{(3-\nu)}{2} - \frac{2(1+\nu_b)}{E_b}}. \end{aligned} \quad (2)$$

where E_b and ν_b are the Young modulus and Poisson ratio of the base material. For the case of $\phi = 1$, expressions (1,2) are reduced to

$$\begin{aligned} 0 &< \kappa < \kappa_b, & 0 &< \mu < \mu_b, \\ E(\nu) &< -\frac{E_b}{1-\nu_b}\nu + \frac{E_b}{1-\nu_b}, & E(\nu) &< \frac{E_b}{1+\nu_b}\nu + \frac{E_b}{1+\nu_b}. \end{aligned} \quad (3)$$

Note that the rational transformation between (κ, μ) and (E, ν) coordinates is not globally one-to-one: in the extreme case of vanishing Young modulus, both κ and μ go to zero, so the lower side of the triangle in (E, ν) domain collapses to a single point $\kappa = 0$, $\mu = 0$, except points $\nu = \pm 1$. These two points in (E, ν) coordinates correspond to the lines $\kappa = 0$ and $\mu = 0$ in (κ, μ) coordinates. This in part explains why we view (E, ν) coordinates as more intuitive: for low E , there is a substantial difference in measurable behavior between, *e.g.*, materials with $\nu = -1$, and $\nu = 1$, while both κ and μ are close to zero.

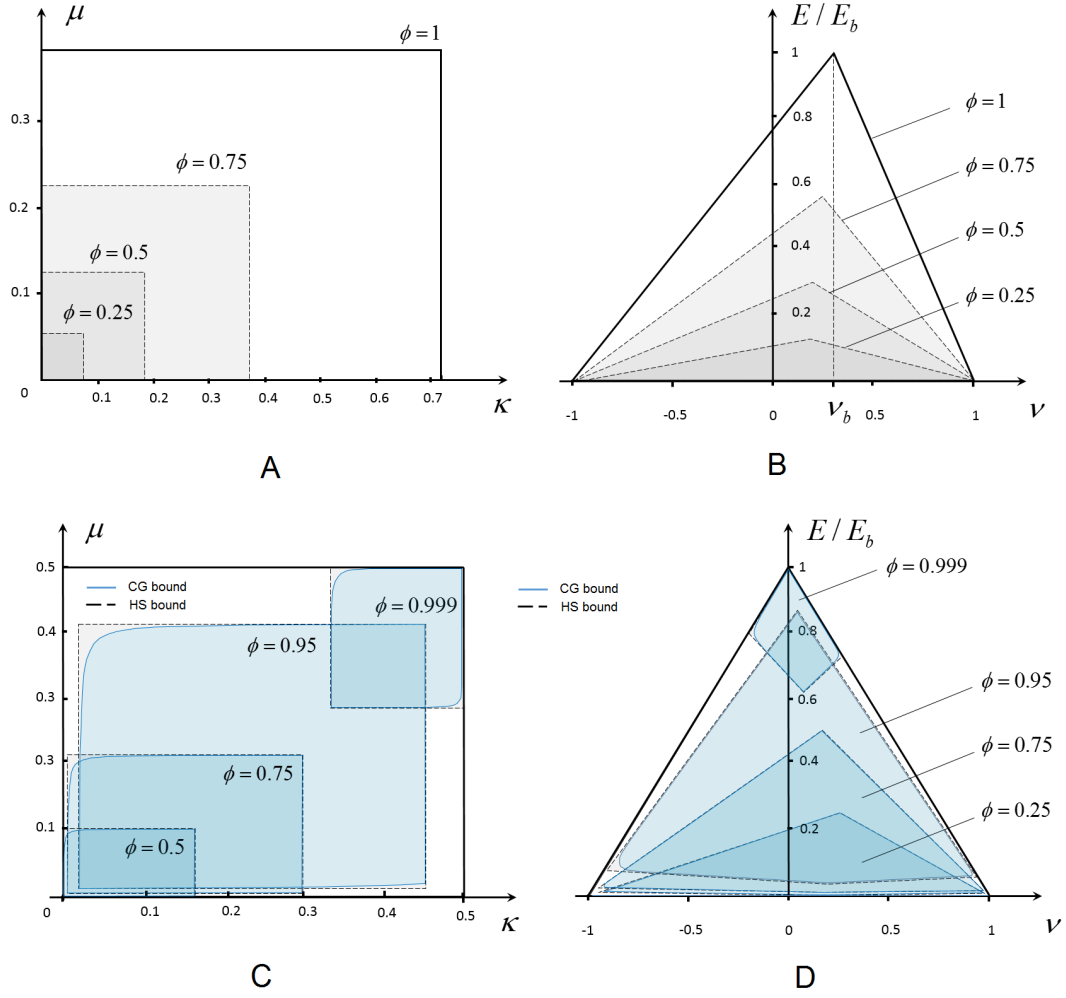


Figure 2: (A, B) Hashin-Shtrickman bounds for the elastic moduli of isotropic void-material composites: (A) in bulk and shear modulus coordinates and (B) the same bounds transformed to Poisson ratio and Young modulus coordinates. (C,D) Hashin-Shtrickman (grey) and Cherkhev-Gibiansky (blue) bounds for elastic moduli of isotropic bimaterial composite ($\nu_s = \nu_w = 0$, $E_w = 0.001E_s$) (C) in terms of bulk and shear moduli and (D) in terms of Poisson ratio and Young modulus. For brevity, here and below Hashin-Shtrickman bounds are labeled on images as HS bounds and Cherkhev-Gibiansky bounds – as CG bounds.

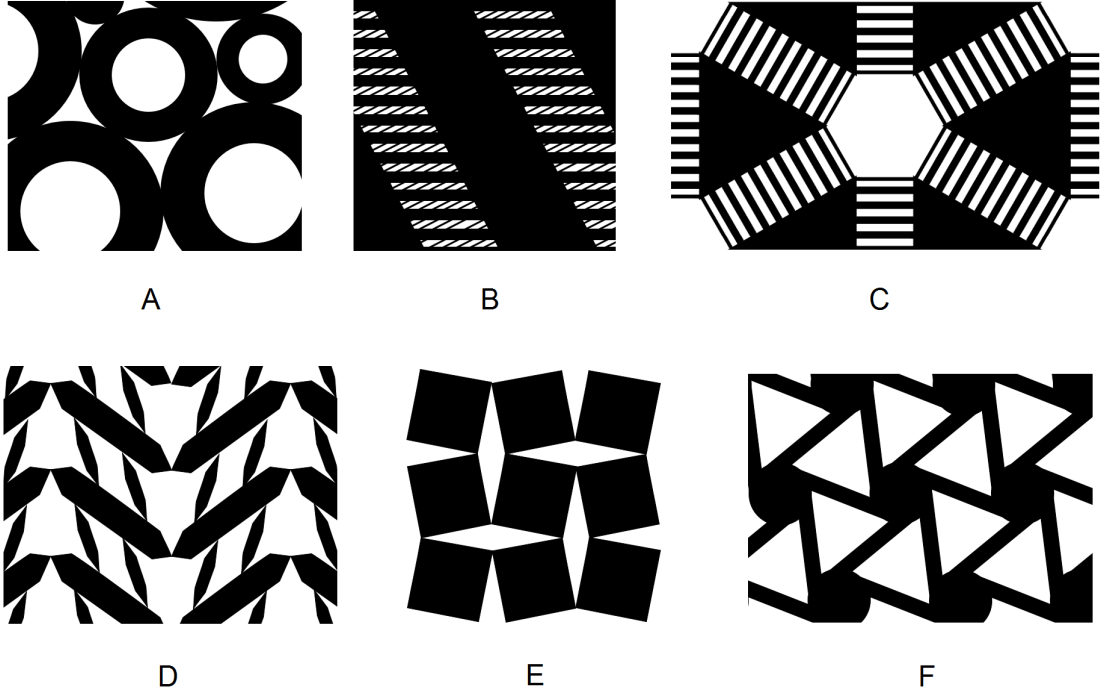


Figure 3: Known extremal composites (A) Coated spheres assemblage, exhibiting extremal bulk modulus, (B) rank 3 sequential laminate, exhibiting maximum bulk and shear modulus (C) Sigmund extremal structure, providing maximum bulk and minimum shear modulus (D) “Herringbone” structure by Milton, providing Poisson ratio of -1 (E) Auxetic material made of rotating squares [5] (F) Chiral isotropic auxetic material[18].

G-closure. The problem of G -closure was extensively studied, and is known to have a solution for thermal properties; however, for elasticity, much less is known. The first theoretical example of a composite attaining maximum bulk modulus, a random assemblage of coated spheres (Figure 3(A)) – was identified by Hashin [6]. Later several authors [11, 15, 3, 12] demonstrated that sequential laminates can achieve extreme bulk and shear modulus simultaneously (Figure 3(B)). Milton and Cherkaev [13] have demonstrated the attainability of G -closure for infinitely rigid and void phases. They describe an approach for constructing composites with any given tensor using elementary structures as building blocks (an example of such structure is given in Figure 3(D)). For the same purpose Sigmund adopted laminated regions, and suggested [20] earlier unknown class of extreme isotropic composites (Figure 3(C)), that display high bulk modulus while maintaining low shear modulus. Our approach is based on this work.

An important related direction is the design of materials with negative Poisson ratio (also known as *auxetic*, or *dilational*). Auxetic materials were first described in the work of Lakes [8], and developed in many papers (see a recent review [9]). Many different types of auxetic materials were identified: *e.g.* unimode structures [13], *e.g.* a herringbone structure presented in Figure 3(D), structures based on rigid rotating units, connected with hinges [4], [5] and honeycomb chiral auxetic structures [18]. We use this idea in our construction.

Topology optimization was used for the purpose of extremal material design (see [22] for an overview). New periodic structure designs were obtained in [19, 14, 21]. However, the problem of finding a structure with specific properties is highly nonconvex; as a result, the optimization often fails to reach the target properties. Use of filtering techniques for suppression of checkerboard effects makes it difficult to obtain complex-topology designs which appear to be necessary for target parameters close to the theoretical bounds. Shape optimization is often more successful at achieving specific target material properties, but topology

preservation means that initial design topology needs to be obtained by other means.

Wide use of additive fabrication lead to renewed interest in using small-scale structure to achieve specific material behaviors: on the one hand, additive fabrication makes fabrication of these complex structures possible; on the other hand, these structures allow to manufacture strong parts with lower weight, or objects with continuously variable material properties, *e.g.*, for manufacturing prosthetic devices, or for “soft” robotics. In this context, a number of additional practical issues become of importance – printability of the structure, the absence of extreme stress concentrations that lead to structure damage, its stability towards unwanted nonlinear behavior. Panetta and co-authors [16, 17] present a framework for the structural design based on ground state search for topology with subsequent low-parametric shape optimization to achieve the desirable elasticity tensor while satisfying a set of additional constraints (*e.g.* constraint on maximum von Mises stress).

Rather than using topology or shape optimization to solve the problem of G-closure numerically, we opt for an intermediate approach: we integrate features of several proposed structures into two parametric families with a small number of parameters. As a result, the material property space coverage of these structures can be explored in brute-force way by parameter sweeps. This achieves two goals: first, allows us to find an inner bound on the G-closure domain (with Hashin-Shtrikman bounds providing the outer domain).

3. Periodic structure families

Our families are based on synthesis of hexagonal/triangular isotropic structures invented by Sigmund [20] (Figure 3(C)), and the chiral structures proposed by Prall and Lakes [18] (Figure 3(F)) for negative Poisson ratio.

Figure 4(A,B) shows the main proposed new periodic structures. The starting point is the Hexagon and Triangle structures presented in [20]. These structures consist of triangular or hexagonal solid areas, connected by rectangles partitioned into separate beams (we refer to these rectangles as laminate areas). We extend these structures in a very simple way, by allowing the beams of laminate region to have arbitrary orientation – this considerably extends the range of materials represented by the structure, providing auxetic behavior via the mechanism described in [18]. Structures of this type are described by four parameters shown in the figure (size of the solid region p_1 , width of the laminate area p_2 , period of the beams in the laminate area p_3 , and width of a beam p_4 , with each dimension measured relative to the previous (*e.g.*, p_2 is a fraction of p_1 , in the range $0 \dots 1$). It is important to note that all parameters are *continuous*, including the one determining the number of beams p_3 ; if it is not of the form $1/n$, where n is an integer, the resulting structure has thinner “remainder” beams, which we place on the sides of the laminate area. In this way, all parameters can be changed continuously, and optimized more easily.

We also consider a limit case of these structures, to provide a validation of the hypothesis that with the number of beams in the laminate areas going to infinity (*i.e.*, the resulting structure becomes two-scale), the material properties approach the boundary of the reachable domain (Figure 4(C)); these structures are parametrized in a similar way, but have only three parameters, as the beam period approaches zero. Parameter p_1 is defined in the same way as for finite structures, and the two remaining parameters θ and α (shown in Figure 5(B) below), define the volume fraction and the orientation angle of the laminated areas. Parameters α and θ are used to set the elastic tensor in the laminated region.

4. Methods

In order to perform the parametric studies of the new periodic structures, we use a FEM-based, regular-grid homogenization code, extending [22]. Our algorithm of periodic homogenization follows the method of mutual energies, as described in [22]. The homogenized tensor of elasticity of the rectangular cell $Y \in \mathbb{R}^2$ is found as:

$$C_{ijkl}^H = \frac{1}{|Y|} \int_Y C_{pqrs}(y) \varepsilon_{pq}^{A(ij)}(y) \varepsilon_{rs}^{A(kl)}(y) dY. \quad (4)$$

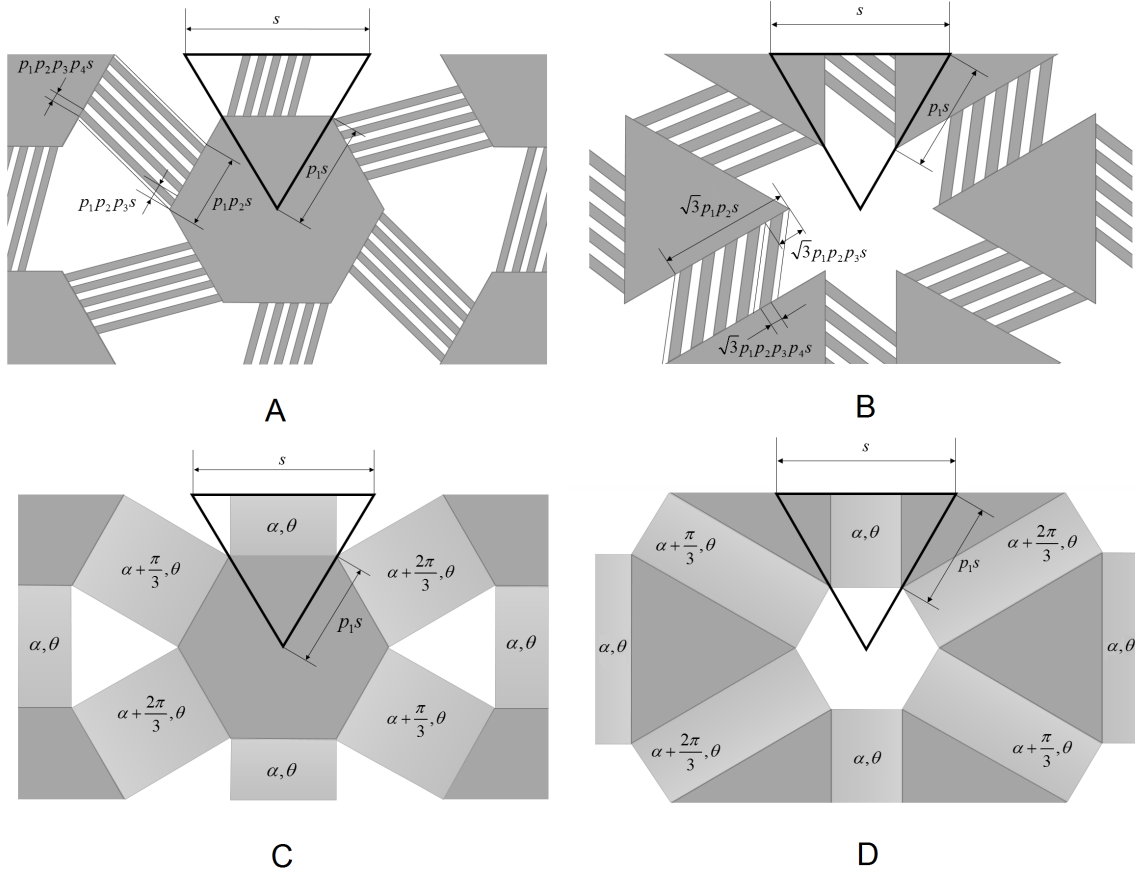


Figure 4: Structure families (A) Triangle, (B) Hexagon (The names follow[20]). (C) Limit structure (only Hexagon structure is shown)

Here $|Y|$ is the area of the cell, $C_{pqrs}(y)$ is the tensor of elasticity of the material at the point y inside the cell domain, and $\varepsilon_{pq}^{A_{ij}}(y)$ are the strain fields induced by the imposition of three constant macroscopic unit test strains A_{ij} . These strains are found by solving three ($pq = 11, 22, 12$) cell problems:

$$\begin{aligned} \left(C_{ijkl}(y) \varepsilon_{kl}^{A_{pq}}(y) \right)_{,j} &= 0, \\ \varepsilon_{kl}^{A(pq)}(y) &= w_{kl}(y) + A_{kl}, \\ w_{kl}(y) &\text{is } Y\text{-periodic.} \end{aligned} \quad (5)$$

Constant unit test strains A_{pq} are imposed on the domain boundary in the form of periodic boundary conditions on displacements u_i^{k+}, u_i^{k-} in the elements nodes (Figure 5(A)):

$$u_i^{k+} - u_i^{k-} = A_{ij}(y_j^{k+} - y_j^{k-}) = A_{ij} \Delta y_j^k. \quad (6)$$

Here $k = 1, 2$ stands for the domain boundaries perpendicular to the k -th coordinate axis. The homogenized elasticity tensor is found as follows:

$$C_{ijkl}^H = \frac{1}{|Y|} \sum_{e=1}^N \mathbf{u}_e^{A_{ij}} \mathbf{k}_e(\mathbf{u}_e^{A_{kl}}), \quad (7)$$

where index e stands for the element, \mathbf{k}_e is the element stiffness matrix, and $\mathbf{u}_e^{A_{ij}}$ is the vector of displacements at the nodes of e -th element upon imposition of A_{ij} -th test strain.

The computational domain is the rectangle comprising $N = N_1 \times N_2$ 4-node isoparametric finite elements (Figure 5(A)). For every element, we specify its density ρ and the type and parameters of its stiffness matrix \mathbf{k}_e . Finite element stiffness matrix $\mathbf{k}_e(D)$ is computed based on the material elasticity tensor in matrix notation D , which is the elasticity tensor.

For finite structures, we use isotropic elasticity tensor.

$$D(E, \nu) = \frac{\rho}{1 - \nu^2} \begin{pmatrix} E & \nu E & 0 \\ \nu E & E & 0 \\ 0 & 0 & \frac{E}{2}(1 - \nu) \end{pmatrix}, \quad (8)$$

where E and ν are the Young modulus of either the strong or weak material (the void is approximated with a very weak material).

To explore the limit case as the genus of the structure goes to infinity, because we increase the number of parallel beams in a particular region, we use the anisotropic rank-one laminate tensor [1].

$$\begin{aligned} D(\alpha, \theta, E_m, E) &= \rho T(\alpha) L(\theta, E_m, E) T^T(\alpha), \quad \text{where} \\ L(\theta, E_m, E) &= \begin{pmatrix} (1 - \theta)E_m + \theta E & 0 & 0 \\ 0 & \frac{1}{\frac{\theta}{E_m} + \frac{1 - \theta}{E}} & 0 \\ 0 & 0 & \frac{1}{2(\frac{\theta}{E_m} + \frac{1 - \theta}{E})} \end{pmatrix}, \\ T(\alpha) &= \begin{pmatrix} \cos^2 \alpha & \sin^2 \alpha & -2 \sin \alpha \cos \alpha \\ \sin^2 \alpha & \cos^2 \alpha & 2 \sin \alpha \cos \alpha \\ \sin \alpha \cos \alpha & -\sin \alpha \cos \alpha & \cos^2 \alpha - \sin^2 \alpha \end{pmatrix}. \end{aligned} \quad (9)$$

In this equation, α is a lamination direction, E_m is the Young modulus of the laminate's soft material (in void-material simulations $E_m = 10^{-6} \cdot E$), θ is the volume fraction of the laminate's strong phase (Figure 5(B)).

We ensure that the effective elasticity tensor obtained by homogenization is isotropic, by using hexagonal/triangular cells, and imposing symmetries of structures with respect to $\pi/3$ rotations, as any elasticity tensor invariant with respect to these symmetries is isotropic [10]. It is important to note that reflectional

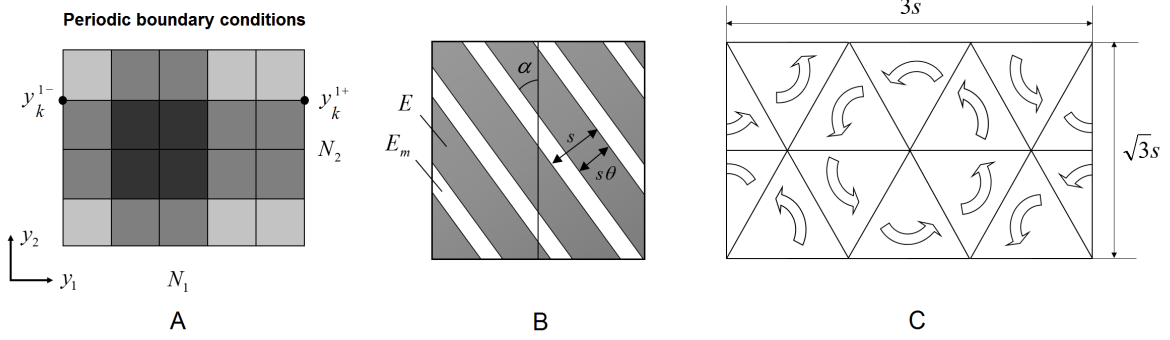


Figure 5: Diagrams of (A) a cell computational domain (B) rank-1 laminate (C) prescribed rotational symmetries of a computational domain.

symmetries are *not* required for isotropy. This makes it possible for us to use *chiral* structures to create isotropic materials.

We use a rectangular computational domain with the ratio of the sides $3 : \sqrt{3}$ (Figure 5(C)). This rectangular base cell has the area of two hexagonal base cells.

The structures studied in this work are defined as unions of polygonal primitives. These are discretized on a regular grid, which is used for FEM discretization. Each square element overlapping the structure is assigned elasticity tensor of the base material (or laminate, if this part is marked as laminate area), scaled by the ratio of the area of the element covered by the structure to the total cell area. This approach improves accuracy, compared to digitizing with only base material elasticity tensor, or void, similar to the way images of sharp boundaries are improved by antialiasing.

For the verification purposes, our computations were also checked with an alternative homogenization tool [16], which is based on representing the shape as an implicit function, and meshing the domains with an unstructured triangular mesh. These two approaches yield close results.

Our homogenization and structure generation codes are available at https://bitbucket.org/iostanin/pco_toolbox_matlab.

5. Numerical studies

We explore the coverage of the families of structures described above using homogenization under several scenarios, as well as provide evidence, using shape optimization, that the boundary we obtain is likely to be close to optimal. For simplicity and ease of understanding, we use a base material with Poisson ratio $\nu_b = 0$. The specific value of E_b simply sets the scale, as we use linear elasticity, so in all plots we use the ratio E/E_b for the effective Young modulus E . The qualitative behavior is similar for different values of ν_b , but the coverage cannot be obtained by a simple transformation.

We define *coverage* of a family of structures as the set of points in effective material properties space (typically in (E, ν) coordinates) that can be obtained for a particular choice of structure parameters. In order to quantify coverage, we introduce coverage coefficients Δ_R, Δ_L , defined as ratios of the highest (lowest) achievable Poisson ratio at $E/E_b = 0.5$, and the corresponding theoretical limit value of Poisson ratio at $E/E_b = 0.5, \phi = 1$ (in case of $\nu_b = 0$, these limit values are $\nu_R = 0.5$, and $\nu_L = -0.5$).

Figure 6(A, B) shows the coverage we were able to obtain with two structure families (Hexagon and Triangle). Figure 6(A) provides the areas covered by two structures, whereas Figure 6(B) shows raw datasets. For comparison, we also sketch the approximate positions of several known extremal composites, shown in Figure 3. Figure 6(C) gives an idea how the coverage depends on the number of beams $n = 1/p_3$ for single scale structures (see the discussion below).

Relatively few papers attempted to design families of structures with a large coverage area. The best coverage known to us was obtained in [17] in 3D. For comparison, we applied the same approach to two-dimensional structures with square symmetries, to estimate coverage that can be compared to the families of structures considered in this paper.

More specifically, a ground structure was obtained by subdividing a square into smaller squares and triangulating each of these. These ground structures are parametrized by node sizes and displacements. Initially, a combinatorial search is performed by removing edges from the ground structure (while maintaining the square symmetries) and generating a set of initial structures that are estimated to yield the largest range of material properties. Then the parameters of each identified structure are optimized multiple times, to minimize the deviation of the homogenized material properties from a set of target pairs (E_i, ν_i) in the admissible region. This optimization is performed by solving the adjoint equations of elasticity at every step to compute the shape derivative. The topology of each structure remains fixed during the optimization.

Figure 6(D) gives the comparison of the performance of our new structures with the ones found previously by ground-state combinatorial search with subsequent shape optimization which provided the widest coverage known so far. We use coverage data for two structures, shown in the same figure, that cover essentially the whole domain covered by any structure obtained by edge removal. We can see that our new Triangle and Hexagon structures ($n = 30$) significantly improve the coverage of possible elastic properties of composites for the same base material's elastic moduli.

Optimality of Hashin-Shtrickman bounds for positive Poisson ratios. Our results provide compelling numerical evidence that Hashin-Shtrickman bound for non-fixed volume fraction can be approached with good precision with Hexagon structures as the number of beams n approaches infinity ($n = 1/p_3$). This is confirmed using simulation with limit laminate structures, which approach the boundary very closely. Figure 7(A) demonstrates the increase of coverage with increase of n , figure 7(B) demonstrates the limit case of the structures with $\phi \rightarrow 1, n \rightarrow \infty$, achieving right Hashin-Strickmann bound. Figure 7(C) indicates that limit laminate structures also remain very close to Hashin-Shtrickmann bound for volume fractions smaller than 1 (see also Figure 10). These results are consistent with the ones obtained previously in [20].

We observe that chirality (captured by the parameter p_2 , or α for a limit two-scale structure) does not play a major role in this case, *i.e.* the right Hashin-Shtrickman bound is closely approximated by structures with no chirality.

The stiffness of such structures (for the considered case $\nu_b = 0$ – the position (E, ν) on $E + \nu u = 1$ straight line) is defined solely by the stripe's relative thickness (p_4 for type one structure and θ for the limit two-scale structure).

Best achievable bound for negative Poisson ratios. Introduction nonzero chirality leads to a decrease of the effective Poisson ratio due to rotation of solid segments of the structure (Figure 8). Extremal values that closely approach left theoretical bound (Figure 9(A)) are provided by the Triangle structure, which is, in a sense, a geometric dual of the Hexagon structure. Similarly to the right bound, increasing the number of beams in the laminate area leads to structures closer to the boundary (Fig. 6(C)). However, in this case, the limit structure does *not* follow the boundary. Figure 10(B) demonstrates this coverage coefficient as a function of the volume fraction ϕ . The coverage curve grows rapidly when approaching volume fraction 1. However, reasonable extrapolation indicate that the coverage does not exceed 0.7. Therefore, left Hashin-Shtrickman bound remains unachieved. The angle of chirality α of the extreme structures is always close to $\pi/3$, however, it depends slightly on the Young modulus (Figure 9(C)).

Intermediate volume fractions. Above we could see that our Triangle and Hexagon structures exhibit wide coverage of elastic properties for volume fractions approaching 1. In this paragraph we take a look at the performance of these structures for intermediate volume fractions.

For both Triangle and Hexagon structures the volume fraction is given by:

$$\phi = 2p_4p_1(1 - p_1) + p_1^2, \quad (10)$$

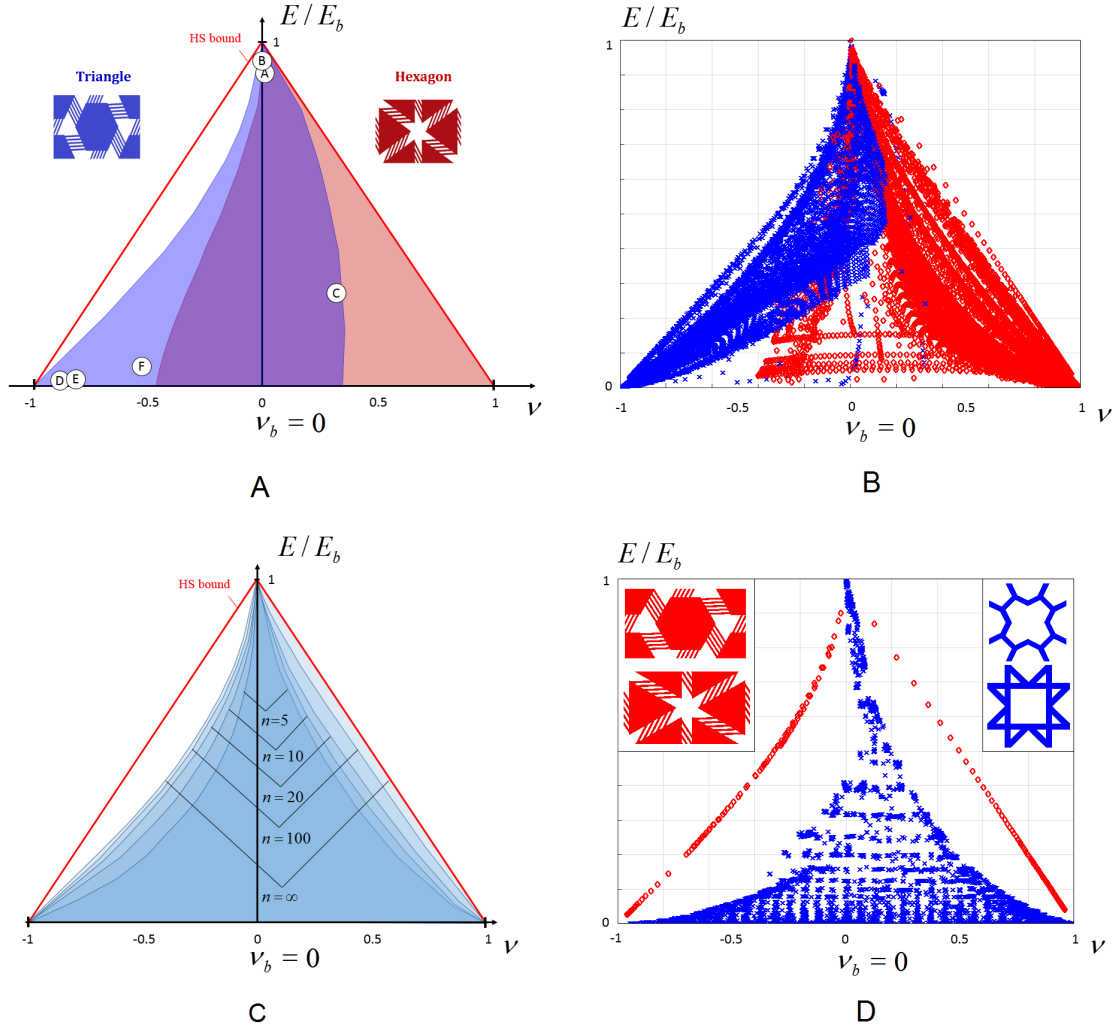


Figure 6: (A, B) Coverage of Hashin-Shtrickman bounds with the new structures of all types. Letters denote tentative positions of the extremal composites presented in Figure 3. (A) -covered sets, (B) - raw data samples. (C) Expansion of the coverage as the number of beams $n = 1/p_3$ increases. (D) Comparison of the coverage obtained in this work with Triangle and Hexagon structures with ($n = 30$, $\nu_b = 0.35$, only extreme structures are shown), in comparison with the widest coverages obtained previously [16]

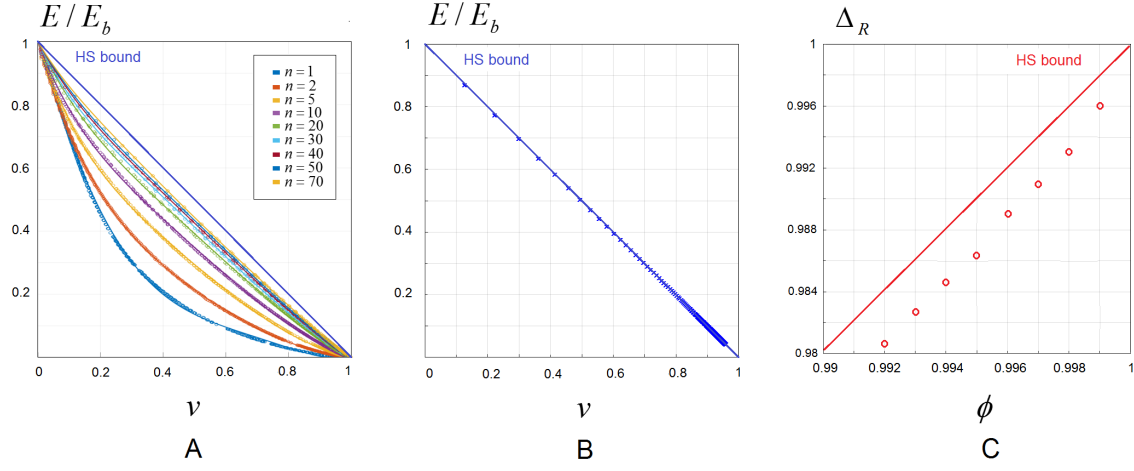


Figure 7: (A) Coverage of elastic properties for positive Poisson ratios as a function of the number of beams in the joint (B) Coverage achieved in the limit case of two-scale structure (C) coverage measure Δ_R as a function of volume fraction ϕ

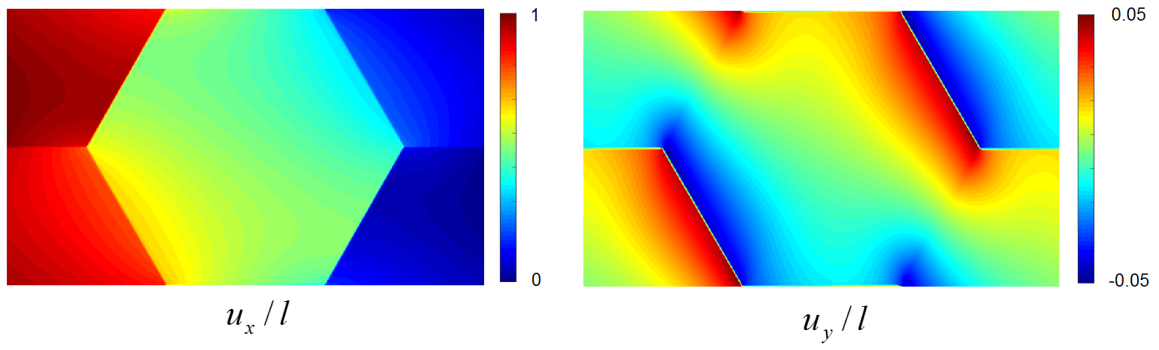


Figure 8: Displacement fields in the horizontal tension ($pq = 11$, “triangle” structure of the second type) cell problem. Rotation of solid parts of the structure, leads to auxetic behavior.

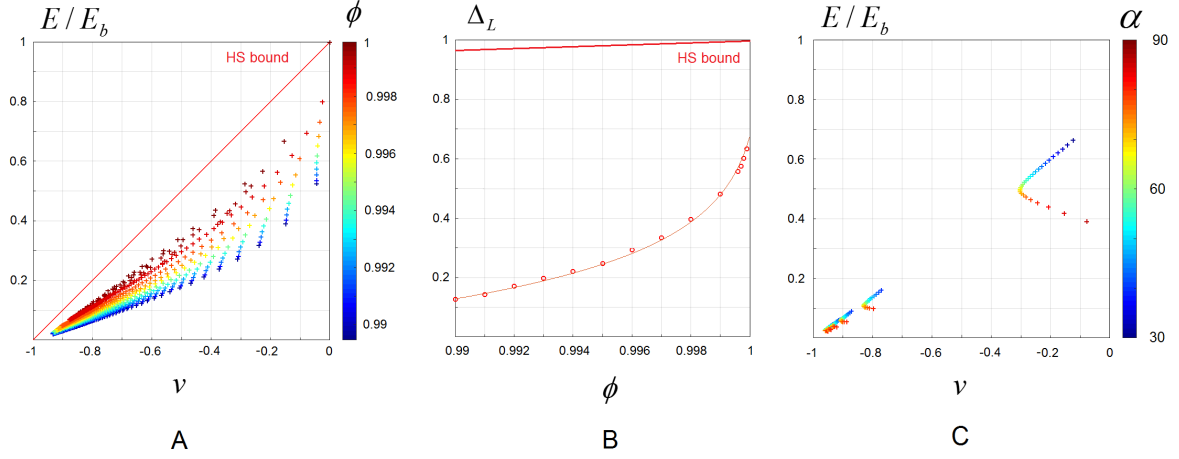


Figure 9: Limit structures approaching left HS bound. (A,B) Left-bound extreme elastic moduli, achieved with the Triangle limit structure; chart colored by values of p_1 (A) and p_2 (B). (C) Dependence of the achievable negative Poisson ratio as the function of chirality angle. Chirality angle p_3 sweeps are performed for several values of p_2 .

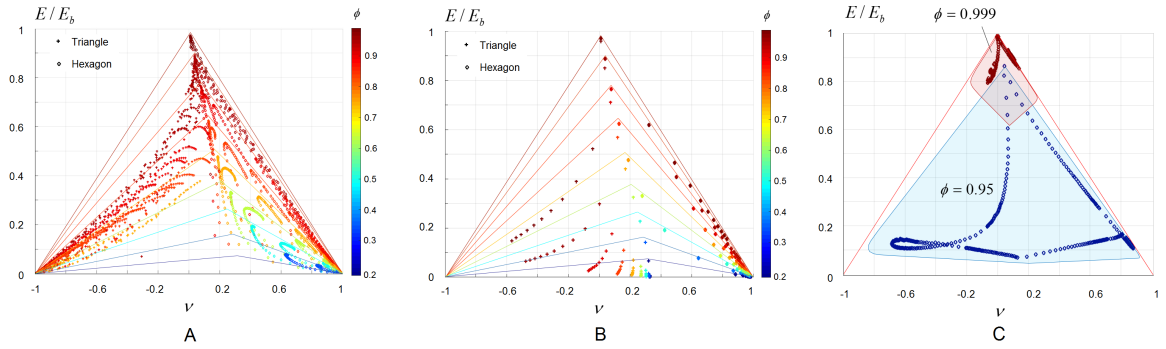


Figure 10: Coverage of Hashin-Shtrickman bounds with triangular and hexagonal structures for a set of intermediate volume fractions. (A) Structures of the first type, (B) structures of the second type. (C) Coverage of Cherkaev-Gibiansky bounds with bimaterial composite for two volume fractions.

or, for the limit two-scale structure,

$$\phi = 2\theta p_1(1 - p_1) + p_1^2. \quad (11)$$

Considering that for the extremal composites $p_4(\theta)$ has to stay very close to 1, the volume fraction can be viewed primarily as the function of a sole argument p_1 .

Figure 10 illustrates the coverage of Hashin-Shtrickman bounds for a set of intermediate volume fractions. Figure 10 (A) gives the parametric sweeps for structures with fixed number of beams, figure 10 (B) demonstrates the behavior of their two-scale counterparts.

For both single scale and two-scale structures, we explored the parameter p_1 in the range $0.1 \dots 0.9$. We can see that in both cases the right Hashin-Shtrickman bound is easily approached with Triangle structures with zero chirality angle, however, the coverage on the left side deteriorates dramatically with decrease of the base material volume fraction. This effect has trivial explanation. Consider the case of two-scale limit structure. Clearly, if $\theta < 1$ and the lamination angle is steeper than the diagonal of the rectangular joint region, the stiffness of the joint drops to zero. Therefore, for the values of p_1 smaller than the critical value defined by

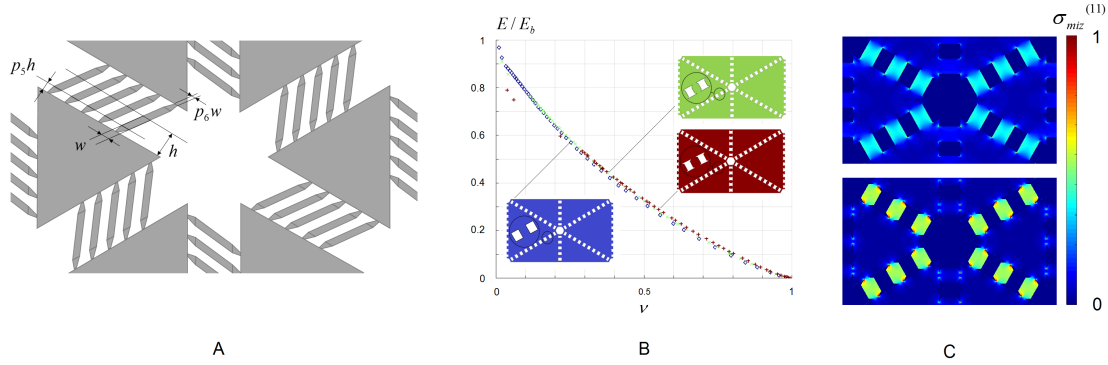
$$\sin \alpha = \frac{p_1}{\sqrt{3(1 - p_1)^2 + p_1^2}}, \quad (12)$$

the stiffness of “triangle” structure will drop to zero. In our case $\alpha = \pi/6$, critical value of $p_1 = 0.5$, and the corresponding volume fraction $\phi = 0.75$. As we can see in Figure 10(B), all the structures with such volume fraction and $p_2 < 1$ have nearly zero stiffness, with the remaining response conditioned by the nonzero density of the ersatz material.

Non-void weak material. In case of a bimaterial mixture, the range of the elastic properties that could be achieved with our structures shrinks significantly compared to the corresponding theoretical bounds. Figure 10(C) gives the coverage achieved for the composite material with the weak phase 1000 times softer than the strong phase. For these cases we performed same parameter sweeps that provided us the most extreme properties in the case of void-material composite. We can see that though the structures without chirality remain close to right bound, the chiral bimaterial structures are very far from the extreme properties.

Expanding the parameter space. Natural question to ask if the expansion of the parameter space will improve the performance of our structures. One obvious way to improve the performance is to modify the configuration of joints, that are supposed to be very strong in axial compression, but very compliant in shear. The performance of the joints can be improved by introducing “intent” regions at the toes of the joint beams (Figure 11(A)). In our numerical experiments the structures with indented beams can not help improving the coverage of the elastic moduli at large volume fractions, since the features of sharpened stripes simply can not be resolved. However, they can be useful for the case of intermediate volume fractions – low values of shear modulus can be reached at lower definition of the structure (*i.e.* smaller number of stripes), which can be important in practical situations. Figure 11(B) illustrates the improvement of the coverage achieved with the structures of second kind over the ones of a first kind. However, this relatively insignificant improvement comes with a cost – higher stress concentrations at the toes of the stripes, that make failures more likely (Figure 11(C)).

Optimality of the negative Poisson bounds. It is difficult to establish with certainty that no points closer to the Hashin-Shtrickman bounds can be found. However, it is highly likely that a very different structure would be needed for this. To validate this conjecture numerically, we have performed the following numerical experiments. Starting from a structure with effective elastic parameters far away from the achievable boundary (but of sufficiently large number of beams), we vary the parameters of the structure to optimize the goal functional. We consider the functional $\|S - S_0\|_F$, the Frobenius norm of the difference between the effective elasticity tensor of our structure, and a target tensor S_0 , which we take to be a point on the Hashin-Shtrickman boundary $(-0.5, 0.5)$. We optimize this functional until the point reaches a minimum which is on the achievable boundary. At this point, the gradient of the functional, with respect to the structure parameters, is zero (or, rather, its projection on the hyperplane orthogonal to the constraint gradients). This



(A) Expanding parameter space: a parameterization of the structure with indented beams.

Figure 11: (B) Change in coverage with addition of indentations. (C) Von Mises stress concentrations caused by the introduction of beam indentations.

N	$\ \nabla\ _\infty$	N	$\ \nabla\ _\infty$
1	172.64	11	19.24
2	170.82	12	18.65
3	169.76	13	13.73
4	168.05	14	13.67
5	165.05	15	10.15
6	117.15	16	10.37
7	90.77	17	8.78
8	90.54	18	9.00
9	51.56	19	9.03
10	31.42	20	8.67

of course, does not imply optimality, as we are considering only a small number of parameters. However, we can measure the norm of the shape derivative with respect to *positions of all points on the shape boundary*. These values are tabulated in Table 5, as a function of the iteration number. We see that close to the boundary the derivative declines by more than an order of magnitude. Examining the distribution of nonzero values, we see that these are almost entirely close to sharp corners of the structure, and are close to zero elsewhere. This suggests that adding degrees of freedom to optimization is not likely to improve how close one can get to the Hashin-Shtrickman bound for negative Poisson ratios. The bound we observe appears to be very close to a local optimum for the family we consider. A radical change in topology would be needed for further improvement.

6. Discussion, conclusions and future work

In our work we have demonstrated nearly complete G-closure for positive Poisson ratio – effectively, attainability of Hashin-Shtrickman bounds for the elastic properties. While for negative Poisson ratio we have not reached the bound, and it remains unclear whether Hashin-Shtrickman bounds are optimal in this case, presented family of structure has broader coverage than any previously considered family.

The region that is left not covered by our structure is the neighbourhood of the left HS bound with values of Young modulus close to 0.5. A number of alternative approaches (*e.g* topology optimization) did not allow us to reach the extremal composite that would attain an isotropic elastic tensor in that region. The questions of the existence of such microstructures, as well as the optimality of Hashin-Shtrickman bounds in that neighbourhood remains unanswered.



Figure 12: Possible generalizations of the extremal structures. (A) Structure with an improved strength due to elimination of stress concentrations (B) Structure with wide coverage of elastic moduli at intermediate volume fractions.

The range of achievable elastic properties available with our two microstructures covers all known two-dimensional isotropic void-material composites (some of them are shown in Figures 3 and 6(A,D)). We are not aware of the regular isotropic structures, random assemblages or general topology optimization solutions that provide elastic moduli that fall out of the coverage presented in our work. Therefore, our work suggest the most robust solution of the two-dimensional problem of inverse homogenization of void material isotropic composites available today.

The theoretical structures suggested in our work can be adapted for practical usage. For example, sharp corners causing stress singularities can be smoothened out (Figure 12(A)). On the other hand, a straightforward modification of the structure (Figure 12(B)) can dramatically improve the performance of the microstructures with intermediate volume fractions.

Although the microstructures suggested in this work do not allow straightforward generalization of the three-dimensional case, similar ideas (laminar-like regions and chirality) can be used to improve the performance of the earlier developed 3D patterns with programmable elastic properties [16, 17].

7. Acknowledgments

The work was supported by the Russian Science Foundation through grant RSF-15-1100033. I.Ostanin acknowledges the financial support from the Russian Foundation of Basic Research (RFBR) under grant 16-31-60100.

8. References

References

- [1] Allaire, G. (2002). *Shape optimization by the homogenization method*. Springer.
- [2] Cherkæev, A. and Gibiansky, L. (1993). Coupled estimates for the bulk and shear moduli of a two-dimensional isotropic elastic composite. *Journal of the Mechanics and Physics of Solids*, **41**(5), 937–980.
- [3] Francfort, G., M. F. (1986). Homogenization and optimal bounds in linear elasticity. *Archives of Rational Mechanics Analysis*, **94**, 307334.
- [4] Grima, J. and Evans, K. (2000). Auxetic behavior from rotating squares. *J. Mater. Sci. Lett.*, **19**, 15631565.
- [5] Grima, J., Alderson, A., and Evans, K. (2005). Auxetic behavior from rotating rigid units. *Phys. Status Solid. B*, **242**, 561575.
- [6] Hashin, Z. (1962). The elastic moduli of heterogeneous materials. *Journal of Applied Mechanics*, **29**(1), 142–150.
- [7] Hashin, Z. and Shtrikman, S. (1963). A variational approach to the theory of elastic behavior of multiphase materials. *J. Mech. Phys. Solids*, **11**, 127–140.
- [8] Lakes, R. (1987). Foam structures with a negative poisson’s ratio. *Science*, **235**(4792), 1038–1040.

- [9] Lakes, R. (2017). Negative poissons ratio materials: Auxetic solids. *Annu. Rev. Mater. Res.*, **47**, 6381.
- [10] Love, A. (1944). *A treatise on the mathematical theory of elasticity*. Dover publications New York.
- [11] Lurie, K.A., C. A. (1985). The problem of formation of an optimal isotropic multicomponent composite. *Journal of Optimization Theory and Applications*, **46**, 571589.
- [12] Milton, G. (1986). Vol. 1 of ima. In *Modelling the Properties of Composites by Laminates*, page 150174. Springer-Verlag.
- [13] Milton, G. and Cherkaev, A. (1995). Which elasticity tensors are realizable? *Journal of Engineering Materials and Technology, Transactions of ASME*, **117**(4), 483–493.
- [14] Neves, M., Rodrigues, H., and Guedes, J. (2000). Optimal design of periodic linear elastic microstructures. *Comput Struct*, **76**(1), 421–429.
- [15] Norris, A. N. (1985). A differential scheme for the effective moduli of composites. *Mechanics of Materials*, **4**, 116.
- [16] Panetta, J., Zhou, Q., Malomo, L., Pietroni, N., Cignoni, P., and Zorin, D. (2015). Elastic textures for additive fabrication. *ACM Transactions on Graphics*, **34**(4), 135:1–12.
- [17] Panetta, J., Rahimian, A., and Zorin, D. (2017). Worst-case stress relief for microstructures. *ACM Transactions on Graphics*, **36**(4), 122:1–14.
- [18] Prall, D., L. R. (1996). Properties of a chiral honeycomb with a poissons ratio 1. *Int. J. Mech. Sci.*, **39**, 305314.
- [19] Sigmund, O. (1994). Materials with prescribed constitutive parameters: an inverse homogenization problem. *Comput. Struct.*, **51**(17), 2313–2329.
- [20] Sigmund, O. (2000). A new class of extremal composites. *Journal of the Mechanics and Physics of Solids*, **48**, 397428.
- [21] X. Huang , A. Radman, Y. X. (2011). Topological design of microstructures of cellular materials for maximum bulk or shear modulus. *Computational Materials Science*, **50**, 1861–1870.
- [22] Xia, L. and Breitkopf, P. (2015). Design of materials using topology optimization and energy-based homogenization approach in matlab. *Struct Multidisc Optim*, **52**(6), 12291241.